NeuroImage 139 (2016) 259–270

Contents lists available at ScienceDirect

NeuroImage

journal homepage: www.elsevier.com/locate/ynimg

Altered structural connectome in adolescent socially isolated mice

Cirong Liu [a,b,c], Yonghui Li [a], Timothy J. Edwards [a], Nyoman D. Kurniawan [d], Linda J. Richards [a,e], Tianzi Jiang [a,b,c,f,*]

[a] Queensland Brain Institute, The University of Queensland, Brisbane, QLD 4072, Australia
[b] Brainnetome Center, Institute of Automation, Chinese Academy of Sciences, Beijing 100190, China
[c] National Laboratory of Pattern Recognition, Institute of Automation, Chinese Academy of Sciences, Beijing 100190, China
[d] The Centre for Advanced Imaging, The University of Queensland, Brisbane, QLD 4072, Australia
[e] The School of Biomedical Sciences, The University of Queensland, Brisbane, QLD 4072, Australia
[f] Key Laboratory for NeuroInformation of Ministry of Education, School of Life Science and Technology, University of Electronic Science and Technology of China, Chengdu 610054, China

ARTICLE INFO

Article history:
Received 11 February 2016
Revised 11 June 2016
Accepted 18 June 2016
Available online 20 June 2016

Keywords:
Brain network
Connectome
Structural connectivity
Diffusion MRI
Orbitofrontal cortex
Social deprivation

ABSTRACT

Social experience is essential for adolescent development and plasticity of social animals. Deprivation of the experience by social isolation impairs white matter microstructures in the prefrontal cortex. However, the effect of social isolation may involve highly distributed brain networks, and therefore cannot be fully explained by a change of a single region. Here, we compared the connectomes of adolescent socially-isolated mice and normal-housed controls *via* diffusion magnetic resonance imaging. The isolated mice displayed an abnormal connectome, characterized by an increase in degree and reductions in measures such as modularity, small-worldness, and betweenness. The increase in degree was most evident in the dorsolateral orbitofrontal cortex, entorhinal cortex, and perirhinal cortex. In a connection-wise comparison, we revealed that most of the abnormal edges were inter-modular and inter-hemispheric connections of the dorsolateral orbitofrontal cortex. Further tractography-based analyses and histological examinations revealed microstructural changes in the forceps minor and lateral-cortical tracts that were associated with the dorsolateral orbitofrontal cortex. These changes of connectomes were correlated with fear memory deficits and hyper-locomotion activities induced by social isolation. Considering the key role of the orbitofrontal cortex in social behaviors, adolescent social isolation may primarily disrupt the orbitofrontal cortex and its neural pathways thereby contributing to an abnormal structural connectome.

1. Introduction

Social experience is important for normal brain development and plasticity of social animals, particularly during adolescence. Social isolation not only induces stress but also deprives the animal of essential experiences required for normal brain maturation and plasticity (Blakemore and Mills, 2014; Fuhrmann et al., 2015), which have been studied extensively in rodent animal models (Buwalda et al., 2011). Recent studies have begun to examine the effect of social isolation on white matter development: social isolation during the first two weeks post-weaning causes detrimental hypo-myelination in the medial prefrontal cortex (PFC) (Makinodan et al., 2012), and chronic social isolation during adolescence and young adulthood causes similar effects (Liu et al., 2012). However, the effect of social isolation may involve highly distributed brain regions, and therefore cannot be fully explained by a change to a single brain region.

Instead of limiting analysis to particular regions or tracts, we can model the complex system as a large-scale network or connectome that fully describes the structural architecture of the brain (Sporns et al., 2005). Recent advances in diffusion magnetic resonance imaging (dMRI) and tractography have enabled the connectivity profiles of the entire brain to be mapped, and have greatly promoted the exploration of the human structural connectome (Sporns et al., 2005). These dMRI-based studies of the human connectome have deepened our understanding of normal brain development and neurodevelopmental disorders such as depression, schizophrenia, and autism (Griffa et al., 2013; Zuo et al., 2012). In contrast to the multitude of discoveries regarding the human connectome, only one dMRI-based study investigated the maturation of the mouse structural connectome, which quantified the brain changes in connectivity during development and revealed a nonlinear relationship between network measures and age (Ingalhalikar et al., 2015).

In this study, we investigated how social isolation during adolescent development affected brain's structural connectome. We acquired high-

* Corresponding author at: Queensland Brain Institute, The University of Queensland, Brisbane, QLD 4072, Australia; Brainnetome Center, National Laboratory of Pattern Recognition, Institute of Automation, Chinese Academy of Sciences, Beijing 100190, China.
E-mail address: jiangtz@nlpr.ia.ac.cn (T. Jiang).

http://dx.doi.org/10.1016/j.neuroimage.2016.06.037
1053-8119/

resolution *ex-vivo* dMRI from normal-housed controls and socially isolated C57BL/6 mice. Based on dMRI, we created an atlas and performed probabilistic tractography to construct the structural connectome. The structural connectomes of the two groups were then compared *via* graph-theory approaches (network-wise comparisons) (Rubinov and Sporns, 2010) and network based statistics (connection-wise comparisons) (Zalesky et al., 2010). We then investigated the association between properties of the structural connectome and behavioral phenotypes. Finally, we performed tractography-based analyses and histology to examine the white matter tracts that may contribute to the abnormal structural connectome. These comprehensive analyses allow us to fully describe the structural connectome in socially isolated mice and facilitate the understanding of social experience in adolescent brain development and plasticity.

2. Materials and methods

2.1. Animals

Thirty-two C57BL/6 mice (18 males and 14 females) were divided into two groups: control (C; 10 males and 7 females) and socially isolated (I; 8 males and 7 females). Mice in the control group were group-housed in standard transparent plastic cages (3 or 4 mice per cage), while mice in the isolated group were housed separately (1 mouse per cage) from postnatal day 35 (P35) for 4 weeks. Behavioral tests were performed from P57 to P61, including an open-field test (1 day), a Y-maze spontaneous alternation test (1 day) and a fear conditioning test (3 days). All mice were housed and handled in accordance with the Queensland Animal Care and Protection Act 2001 and the current NHMRC Australian Code of Practice for the Care and Use of Animals for Scientific Purposes (UQ ethics approval QBI/262/12/RSA).

2.2. Behavioral tests

The open-field test was used to assess novel environment-induced locomotor activity (Walsh and Cummins, 1976). Mice were placed in a transparent cage with the light intensity adjusted to 85 lx (Activity Monitor system, MED Associates, Inc., St. Albans, VT, USA), and locomotion was measured for 2 h using digital counters with infrared sensors. One male socially isolated mouse and 6 female mice (3 controls and 3 socially isolated mice) were excluded from the open field test due the failures of equipment.

The Y-maze spontaneous alternation test was used to assess spatial working memory based on the animal's innate disposition to alternate between arms of the maze (Dember and Fowler, 1958). The Y-maze was composed of three connected transparent acrylic arms (L40 cm × W10 cm × H22 cm) separated by 120°, and visual cues including chairs, rubbish bins, boxes and curtains *etc.* were placed in the room to assist the mice in distinguishing different directions. A camera was positioned above the maze for video recording and the light intensity was adjusted to 85 lx. The test lasted for 8 min and the sequence of arm entries was recorded. The percentage of alternation was the number of trials containing consecutive entries into all three arms divided by the number of all alternations.

The fear conditioning test was used to assess fear memory. Fear conditioning is a form of classical conditioning involving the repeated pairing of a non-threatening stimulus (conditioned stimulus) with an aversive stimulus (unconditioned stimulus) (Maren, 2001). The fear conditioning protocol we employed was similar to a previous study (Pattwell et al., 2011), including one conditioning day followed by two test days. On the conditioning day, mice were placed in a mouse test chamber (Coulbourn Instruments, Whitehall, PA, USA) inside a sound-attenuated box with white walls and an electrified floor grid. After a 2-minute acclimation, mice were conditioned with three pairs of conditioning and un-conditioning stimuli (CS–US) that consisted of a 30-second tone (5 kHz, 70 dB) coincident with a 1-second, 0.7-mA foot shock delivered through the electrified floor grid. Individual pairings were separated by a 30-second inter-trial interval. After the final CS–US pairing, mice remained in the chamber for 1 min before being returned to their home cages. Twenty-four hours later, mice were assessed for contextual fear memory, which was carried out in the same chamber as the conditioning day. Freezing behavior was scored during the 5.5 min in the chamber used for the contextual fear conditioning. Forty-eight hours later, mice were assessed for cued fear memory in a new chamber with black walls and a smooth green plastic floor. After a 2-minute acclimation, mice were presented with three 30-second tones (5 kHz, 70 dB) separated by an inter-trial interval of 30 s. After the last tone, mice stayed in the chamber for 1 min before being returned to their home cages. Freezing behavior was scored during the 30-second tone presentations for the tone (cued) fear conditioning.

2.3. Diffusion MRI data acquisition

After behavioral tests, mice were perfused and prepared for MRI scanning. The animals were anesthetized with lethabarb (VIRBAC PTY, Australia) and perfused with 0.1 M phosphate buffered solution (PBS; BioWhittaker, USA) followed by 4% paraformaldehyde (pH 7.4; Sigma-aldrich, USA) in PBS, and further post-fixed for 24 h. The brain samples were then stored in 0.1 M PBS with 0.02% sodium azide (Sigma-aldrich, USA). Before MRI scanning, the brains were immersed in 0.1 M PBS with 0.2% gadopentetate dimeglumine (Magnevist, Bayer, Leverkusen, Germany) for four days to enhance MRI contrast. Diffusion-weighted magnetic resonance images were acquired using a 16.4T vertical bore, small animal MRI system (Bruker Biospin, Rheinstetten, Germany; ParaVision v5.0) equipped with Micro2.5 imaging gradient and a 15 mm linear surface acoustic wave coil (M2M, Brisbane, Australia). Three-dimensional diffusion-weighted spin-echo sequences were acquired using the following parameters: repetition time = 400 ms, echo time = 20 ms, $\delta/\Delta = 2.5/12$ ms, field of view = 18.99 × 11.16 × 8 mm, matrix = 190 × 112 × 80, bandwidth = 50 kHz, 30 direction diffusion-encoding with b-value = 5000 s/mm^2, 2 b0 images acquired without diffusion-weighting and 0.1 mm isotropic resolution. Acquisition time for one brain was 15 h with 1.5 partial Fourier encoding acceleration in the phase dimensions.

2.4. Construction of structural connectomes

Nodes and edges are two key components of structural connectomes. Below, we first explain how the atlas was constructed to define the nodes (Fig. 1A–B), and then describe how the edges between each pair of nodes were computed *via* probabilistic tractography (Fig. 1C–D).

2.4.1. Atlas construction: defining nodes

The first step of network construction was to define regions of interest (ROIs) as nodes (Fig. 1A–B). Two *ex-vivo* MRI-based atlases of adult C57BL/6 mouse were utilized to create these ROIs: one from the Centre for Advanced Imaging at The University of Queensland (CAI atlas) and the other from the Mori lab of Johns Hopkins University (JHU atlas). The CAI atlas was created using the same 16.4T small animal MRI system as the current study (Ullmann et al., 2013), which provided fine-grained parcellations of the mouse neocortex but lacked the subcortical structures. The JHU atlas provided subcortical structures but the cortex was not parcellated (Chuang et al., 2011). The JHU template (T2 image) was first spatially transformed (affine transformation followed by nonlinear deformation) to the CAI template (T2 image) by Advanced Normalization Tools (ANTs, *http://stnava.github.io/ANTs/*), and then ROIs from the two atlases were merged to form a combined atlas with 78 ROIs (39 on each hemisphere, see Supplementary Table S1) that covered all major cortical and subcortical brain regions. The combined atlas was mapped (affine transfromation followed by nonlinear deformation) to

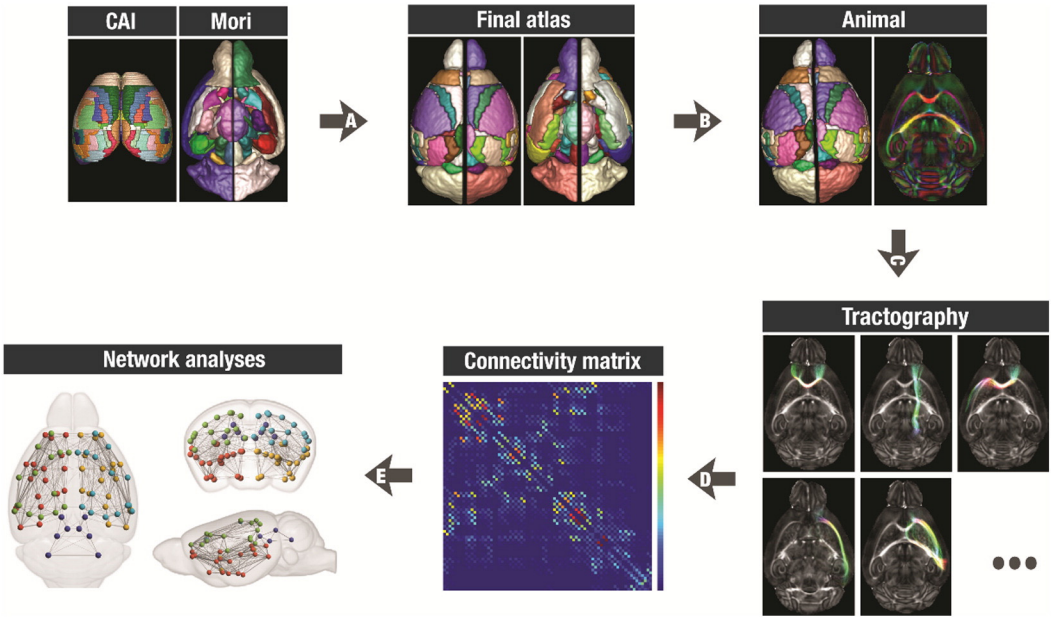

Fig. 1. Flow chart of structural connectome construction. (A) Creating a combined MRI atlas based on the CAI atlas (cortical regions) and Mori atlas (subcortical regions). (B) Transforming the combined MRI atlas to the space of each animal. (C) ROI-to-ROI probabilistic tracking based on the combined MRI atlas. (D) Constructing the connectivity matrix as a structural connectome for each subject. (E) Network analyses and comparisons.

each subject (b0 image) by ANTs and used for probabilistic tractography. As olfactory bulbs of several subjects were damaged during brain extraction, we excluded the olfactory bulbs from the analyses to prevent any bias introduced by the damage. Thus, a total of 76 ROIs were included for probabilistic tractography and connectome analyses.

2.4.2. Probabilistic tractography: defining edges

The second step of network construction was to compute the edges between each pair of nodes *via* probabilistic tractography (Fig. 1C–D). Probabilistic tractography was performed using in-house scripts based on MRtrix2 (*http://www.brain.org.au/software/*), using similar procedures optimized for C57BL/6 adult mice (Calamante et al., 2012; Moldrich et al., 2010). Constrained spherical deconvolution was employed to model multiple fiber orientations in each voxel, with a maximum harmonic order lmax = 6 which determines the 'sharpness' of the fiber orientation distributions (FOD) (Tournier et al., 2007). Probabilistic fiber-tracking was performed using second order integration over the fiber orientation distributions algorithm (step-size = voxel-size/10 = 0.01 mm; curvature values = 0.05). To ensure that tractography was restricted to white matter tracts, any streamline length below 0.5 mm was discarded and the tracking was terminated when fiber orientation distribution amplitude was <0.1. Tracts were generated independently for each pair of ROIs, where one ROI was used as a seed, the other as a target and *vice versa*. Tracking stopped when 5000 streamlines were selected or 500,000 were generated for each tract. The number of streamlines reaching a target region (selected streamlines) divided by the total number of streamlines generated was calculated as the connectivity probability from the seed region (i) to the target region (j). Since probabilistic tractography was performed in both directions (i to j and j to i), the final connectivity probability (weighted edge) of i and j was computed by averaging these two probabilities. These connectivity probabilities composed the structural connectome of each mouse, which was represented as a symmetric 76×76 connectivity matrix.

2.5. Comparison of structural connectomes

Comparisons of structural connectomes between the two groups of mice were performed at the network level by graph-theory analyses (network-wise) and at the individual connection using the network-based statistic (connection-wise). Graph-theory analyses were conducted using the GRETNA (Wang et al., 2015) (*https://www.nitrc.org/projects/gretna/*), and the connection-wise comparisons were performed using the Network Based Statistic Toolbox (Zalesky et al., 2010) (NBS; *https://sites.google.com/site/bctnet/comparison/nbs*).

2.5.1. Network-wise comparisons

Network sparsity was defined as the ratio between the real number of connections and the maximum possible number in a network. As 76 ROIs were involved in the tractography, the max number of connections excluding self-connections would be 5700 ($76 \times 76 - 76$). However, the brain was not a full-connected network, but was a sparse network that had less number of connections than the maximum possible number. Unlike deterministic tracking, probabilistic tractography generated spurious connections with extremely small connectivity probabilities between pairs of unconnected regions. Thus, a threshold was required to identify these false-positive connections before further network analyses. To avoid the bias from one single threshold, the network analyses were conducted using a series of thresholds, ranging from 10% network sparsity ($5700 \times 0.1 = 570$ connections) to 30% sparsity ($5700 \times 0.3 = 1710$ connections), which corresponded to probability thresholds from 0.01 to 0.05 (Supplementary Figure S1).

To compare structural connectomes between the two groups, the following graph theoretical measures were computed under different thresholds (Rubinov and Sporns, 2010).

1) *Degree*. Weighted degree of a node is the sum of edge weights linking to the node. The weighted degrees of all nodes were averaged to obtain the network degree.
2) *Betweenness*. Betweenness centrality of a node is the percentage of all shortest paths that contain the node (Brandes, 2001). The betweenness of all nodes was averaged to obtain the network betweenness.
3) *Small-worldness*. Clustering coefficient measures how nodes in a network tend to cluster together by calculating the fraction of the node's neighbors that are also neighbors of each other (Watts and Strogatz, 1998); and characteristic path lengths measures the efficiency of information transferred on a network by calculating the average

distance between pairs of nodes (Watts and Strogatz, 1998). A small-world network is originally characterized by high clustering coefficient as regular lattices and small characteristic path lengths as random graphs for binary networks (Watts and Strogatz, 1998). The small-world network can be generalized as having high efficiency of information transfer at both the global and local scales (high global and local efficiencies), a concept that is valid for both binary and weighted networks (Latora and Marchiori, 2003). Network global efficiency was calculated as the inverse of the harmonic mean of the shortest path length between all pairs of node. Local efficiency of a node was the global efficiency of the neighbourhoods (subgraph) of the node, and local efficiencies of all nodes were averaged to obtain network local efficiency. Both network global efficiency and network local efficiency were normalized to the corresponding averaged measures of matched random networks that were generated 100 times using the Markov-chain algorithm (Maslov and Sneppen, 2002). The small-worldness was calculated as the ratio between the normalized local efficiency and the normalized global efficiency (Wang et al., 2015).

4) *Modularity*. The structural network can be segregated into several modules or communities. The modularity (Q) measures the difference between the actual number of intra-modular connections and the expected number for the same modules in randomized networks (Danon et al., 2006). Here, we used a greedy optimization algorithm to optimize the network modularity (Clauset et al., 2004; Danon et al., 2006). Generally, networks with high modularity have dense connections within modules, but sparse connections between different modules, indicating a strong partition of the network.

These network measures were calculated for each subject under different thresholds. The effect of isolation on these measures was examined by two-way analysis of variance (ANOVA), where the group factors (control and socially isolated groups) and the threshold factors were fitted to the model. The two-way ANOVA allowed us to examine whether the group factors were significant or not. Meanwhile, the area under a curve (AUC) for each network measure was also calculated to provide a scalar independent of specific threshold selection (Wang et al., 2015). In brief, the AUC was calculated by doing a definite integral between two thresholds (Fig. 2B). The AUC of each network measure and node measure was compared between groups by Welch two-sample *t*-test. Correlations between these network measures and behavioral performance were also analysed. P-values for multiple comparisons were corrected using the Holm–Bonferroni method (Holm, 1979) if and when necessary. All statistical analyses were conducted using R language (*https://www.r-project.org/*).

2.5.2. Connection-wise comparisons

The NBS was used to identify connections that were most affected by social isolation. The NBS is a nonparametric technique to control the family-wise error rate (FWER) when comparing every connection of a network (Zalesky et al., 2010). Although operating directly on raw network matrices, the NBS requires a primary threshold to construct a set of suprathreshold links for later permutation testing. The primary threshold only affects its sensitivities, but not the control of the FWER (Zalesky et al., 2010). A range of primary thresholds were examined from $t = 2.5$ to $t = 3.5$, and the results based on the threshold with the highest statistical significance (the lowest FWER-corrected p-value of any components) were selected for presentation. The patterns of significant connections were examined, and correlations between these connections and behavioral performances were also tested.

2.6. Tractography-based analyses

The above analyses of structural connectome suggested that the forceps minor and the lateral-cortical tracts may be affected by the social isolation (see Results). To reconstruct these tracts, seed regions of interest (ROIs) at the PFC and waypoint/target ROIs were manually drawn on the CAI template (Supplementary Figure S2) and spatially transformed (affine transfromation followed by nonlinear deformation) to each subject (b0 image) by ANTs. Subsequently, ROIs were used to create the streamlines of the forceps minor of the corpus callosum (fmi, Supplementary Figure S2A) and the lateral-cortical tracts (lc, Supplementary Figure S2B). ROIs were independently verified by another investigator with expertise in C57BL/6 mouse brain anatomy and were similar to those used in our previous study (Moldrich et al., 2010). The probabilistic tractography was performed using the same approach as the construction of structural connectome. Each tract was generated independently for each hemisphere and the tracking stopped when 10,000 streamlines were selected for each tract. A series of streamline thresholds (the number of streamlines passing through a voxel) from 25 streamlines to 500 streamlines were used to exclude voxels outside of the tract-of-interest, and the best thresholds were chosen to build a

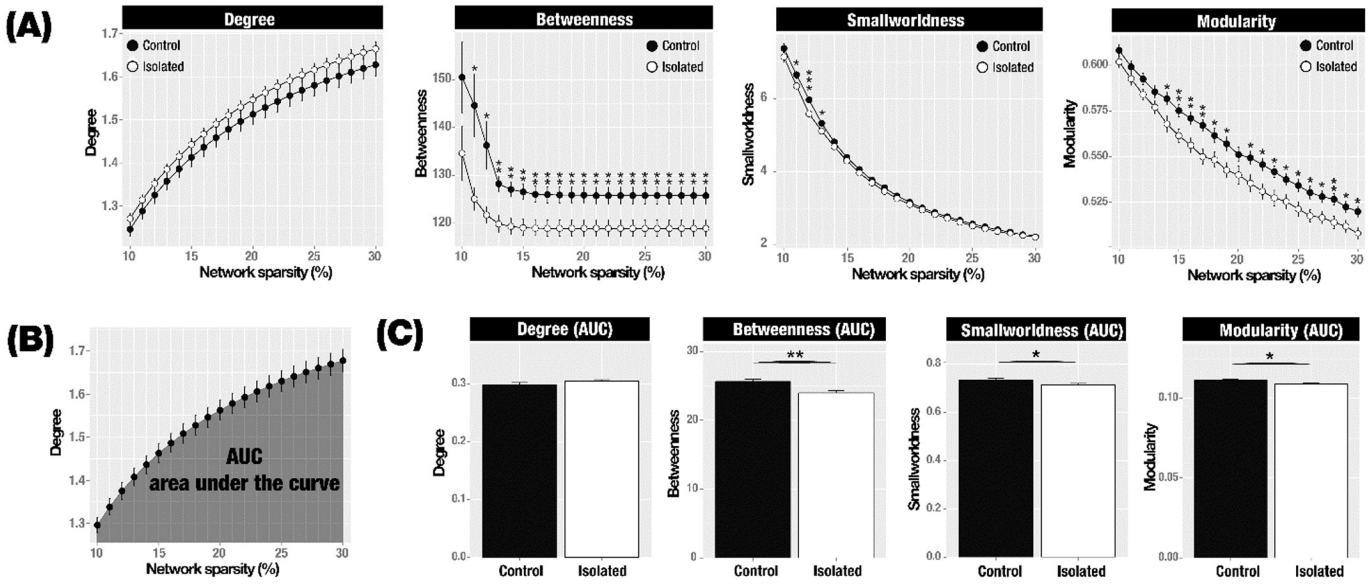

Fig. 2. Network-wise comparison reveals an abnormal structural connectome in socially isolated mice. (A) Network measures across different network sparsities. The structural connectome of socially isolated mice displays an increase in network degree, but reductions in network betweenness, small-worldness and modularity. (B) A demonstration of "area under the curve" (AUC). (C) The AUC of these network measures across all network sparsities. Values are presented as mean ± SEM for each group. $^{*}p < 0.05$, $^{**}p < 0.01$, and $^{***}p < 0.001$.

binary mask for each tract (Supplementary Figure S3). Diffusion-tensor properties, including fractional anisotropy (FA), mean diffusivity (MD), radial diffusivity (RD) and axial diffusivity (AD), were averaged for each tract and compared between the two groups. Comparisons of diffusion-tensor properties using non-optimal streamline thresholds also produced similar patterns to those of optimal thresholds (data not shown). The analyses were performed separately for each hemisphere, expect for the forceps minor where the left and right tracts form one commissural tract.

2.7. Histological examinations

Histology was performed on 7 controls and 6 socially isolated mice (all males). We investigated the densities of total cells (DAPI+), oligodendrocytes (Olig2+/CC1+), as well as myelin content using the intensity of myelin basic protein (MBP+). Fluorescence z-stack images of the forceps minor (Bregma 1.18 mm ± 0.06 mm) for the sections with anti-Olig2 and anti-CC1 antibodies were obtained on a Zeiss Axio Imager with ApoTome using a 20× objective. For the sections with anti-MBP antibody, fluorescence images were obtained using a 10× objective (1 image for each hemisphere per mouse). Images were analysed using FIJI/ImageJ (Schindelin et al., 2012). The densities of total cells (DAPI+) and oligodendrocytes (OLIG2+/CC1+) were estimated using a threshold-based method. For the sections with anti-MBP antibody, the analysis was performed on raw images (without any preprocessing), where the intensity of the fluorescence signals was averaged in the forceps minor. Detailed histological protocols were described in *Supplementary Methods - Immunofluorescence*.

3. Results

3.1. Abnormal structural connectome in socially isolated mice

We constructed structural connectomes of mouse brains (Fig. 1C–D) and examined the effect of social isolation on network measures by two-way ANOVA (Fig. 2A). Socially isolated mice had a higher network degree than controls ($F(1,20) = 29.32$, $p < 0.001$, corrected), suggesting a higher overall connectivity probability in socially isolated mice. Contrary to the degree, socially isolated mice showed significant reduction relative to controls in betweenness ($F(1,20) = 110.44$, $p < 0.001$, corrected), small-worldness ($F(1,20) = 44.36$, $p < 0.001$, corrected), and modularity ($F(1,20) = 122.70$, $p < 0.001$, corrected). The betweenness measures the influence of each node on the information transfer in a network (Brandes, 2001); the small-worldness quantifies the efficiency of information transfer at both the global and local scales (Watts and Strogatz, 1998); and the modularity characterizes the quality of segregating a network into modules or communities (Girvan and Newman, 2002). The changes in these network features indicate an abnormal network structure in the socially isolated mice (Fig. 2A). Similar analyses were also conducted on binary networks, which produced similar results to the weighted networks (Supplementary Figure S4).

We also compared "the area under the curve" (AUC) of these network measures between the two groups using Welch's two-sample *t*-test (Fig. 2C). Consistently, the socially isolated mice had significant reductions in betweenness ($t(29.80) = 3.48$, $p = 0.0064$, corrected), small-worldness ($t(29.98) = 2.23$, $p = 0.033$, uncorrected), and modularity ($t(29.37) = 2.60$, $p = 0.042$, corrected). The degree was higher in socially isolated mice, but not significantly ($t(25.95) = -1.21$, $p = 0.24$, uncorrected) (Fig. 2C).

The group difference in the network degree was relatively small and not as significant as other measures (Fig. 2), suggesting that the high connectivity probabilities may be concentrated between a few nodes. We compared the nodal degree between groups and identified brain regions with significantly higher degree in the socially isolated mice (Fig. 3), including the right dorsolateral orbitofrontal cortex (Dlo.R; $t(25.54) = -4.35$, $p = 0.014$, corrected), entorhinal cortex (Ent.R; $t(25.82) = -4.20$, $p = 0.021$, corrected), and perirhinal cortex (Pr.R; $t(29.98) = -4.38$, $p = 0.010$, corrected). The left parts of these brain regions also had a higher degree in the socially isolated mice, although these measurements did not reach statistical significance.

3.2. Abnormal inter-modular and inter-hemispheric connectivity in socially isolated mice

Network-wise comparisons revealed abnormalities in global and local (nodal) measures, but did not show which connections were affected by social isolation. By using the network based statistics (NBS), we compared each connection of the structural connectome between groups. The connection-wise comparisons unveiled three major patterns (Fig. 4). First, most of the abnormal edges were inter-modular and inter-hemispheric connections, which explain the higher modularity in the socially isolated mice. Second, most of the abnormal edges were connected with the prefrontal regions, especially the dorsolateral orbitofrontal cortex, suggesting that disruptions in the connectivity of the prefrontal cortices may be a major contributor to the abnormal structural connectomes of the socially isolated mice. Third, these abnormal connections had higher weights in the socially isolated mice than in controls, consistent with the network-wise comparisons. These three patterns were consistent under different primary thresholds required for the NBS analyses (Fig. 5).

3.3. Abnormal structural connectomes are associated with abnormal behaviors

We assessed the influence of social isolation on locomotor activity, spatial working memory, and fear conditioning (Fig. 6). Compared with the control group, the socially isolated mice showed significantly higher locomotor activity ($t(19.80) = -2.60$, $p = 0.034$, corrected) in the open-field test, and lower freezing behaviors in both the context fear conditioning ($t(29.43) = 2.89$, $p = 0.022$, corrected) and the tone fear conditioning tests ($t(29.87) = 4.81$, $p < 0.001$, corrected). The socially isolated mice exhibited normal spatial working memory function, as no difference was found in the Y maze spontaneous alternation test ($t(28.88) = 1.11$, $p = 0.28$, uncorrected).

Having observed significant changes in the structural connectome of mice reared in isolation during adolescence, we were interested to investigate whether these changes also correlated with significant behavioral abnormalities induced by social isolation. As shown in Fig. 7A, the modularity was negatively correlated with locomotor activities ($R = -0.70$, $p < 0.001$, corrected), and positively correlated with contextual fear conditioning ($R = 0.51$, $p < 0.005$, corrected) and tone fear conditioning ($R = 0.59$, $p < 0.001$, corrected). These correlations between network property and behaviors suggest that structural connectome was strongly associated with brain functions and behaviors (Fig. 7A).

We further investigated the correlations between abnormal edges (using their connectivity probabilities) and behavioral deficits (Fig. 7B and Supplementary Table S2). Both contextual and tone fear conditioning were significantly correlated with edges that were linked to brain regions implicated in fear memory, including the prefrontal cortices (Dlo, Fra, Vmo), anterior cingulate cortex (Ac), hypothalamus (Hyp), entorhinal cortex (Ent), perirhinal cortex (Pr), ectorhinal cortex (Ect), secondary motor cortex (M2), and primary auditory cortex (*A*1). Similar correlations were also observed for locomotion activities, but were more widespread, with extra edges that linked to the endopiriform nucleus (End), caudate and putamen (Cp), retrosplenial area (Rsp), secondary somatosensory cortex (S2) and secondary visual cortex (V2l). Most of these regions were connected with the prefrontal cortices by abnormal edges, indicating that structural connectivities of the prefrontal regions are important for these behaviors.

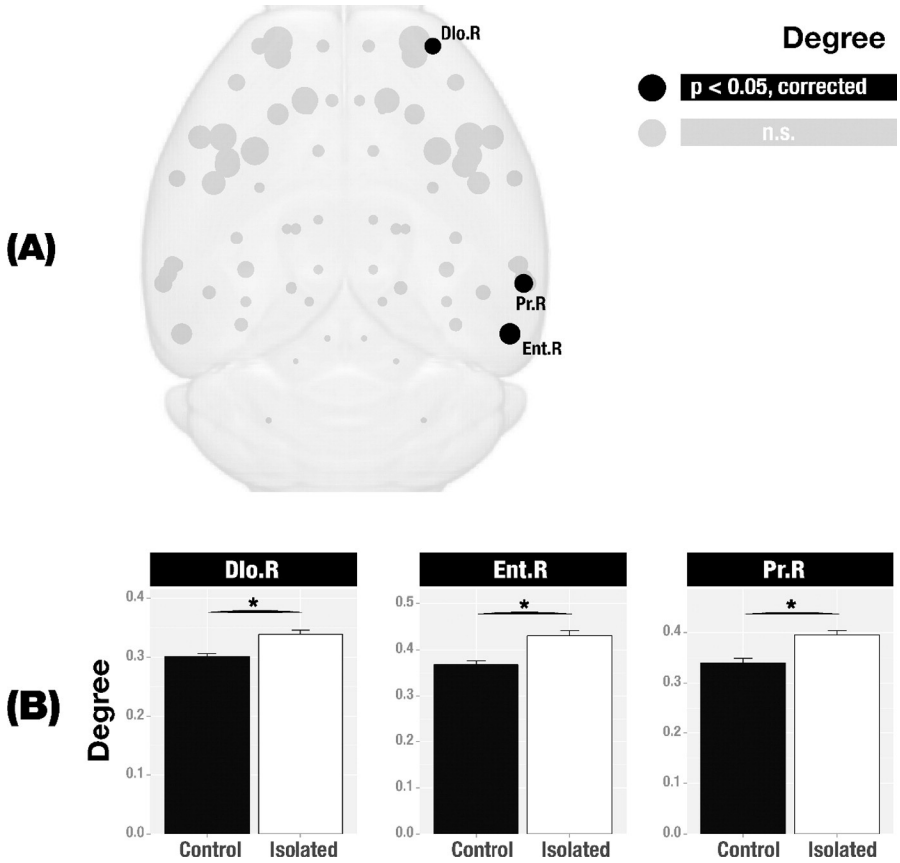

Fig. 3. Significant difference in nodal degree is observed. (A) Socially isolated mice show significantly higher nodal degree (AUC) than controls in the right dorsolateral orbitofrontal cortex (Dlo.R), entorhinal cortex (Ent.R), and perirhinal cortex (Pr.R). (B) Bar graph of the nodal degree (the area under the curve, AUC) in these regions for the two groups. Values are presented as mean ± SEM for each group. *$p < 0.05$.

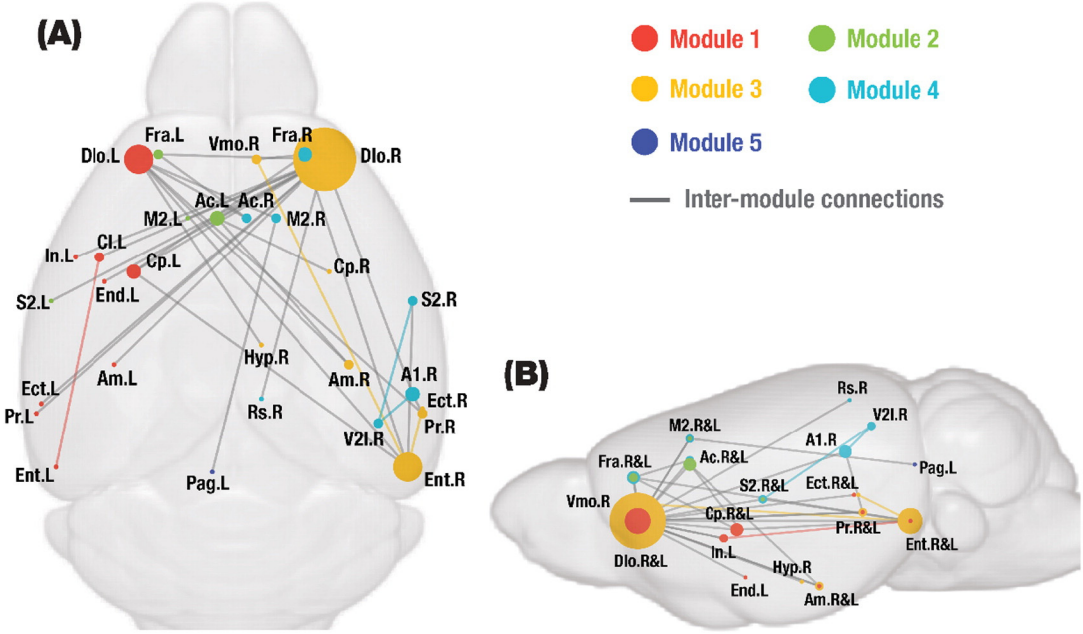

Fig. 4. Connection-wise comparison reveals abnormal inter-modular and inter-hemispheric connectivities in socially isolated mice. (A) The transverse view of the abnormal edges. (B) The sagittal view of the abnormal edges. The Network Based Statistics analysis under the primary threshold ($t = 3.0$) is selected for the presentation, as its result shows the highest statistical significance ($p = 0.016$) (Fig. 5). The size of a node represents the number of abnormal connections associated with that node. The color of a node represents the module to which it belongs. Colored lines are the abnormal within-module connections, and gray lines are the abnormal inter-module connections. All colors are determined by the modularity analysis on the averaged connectivity matrix across subjects, and are used for the purpose of demonstration only. The full name of each abbreviation is listed in Supplementary Table S1.

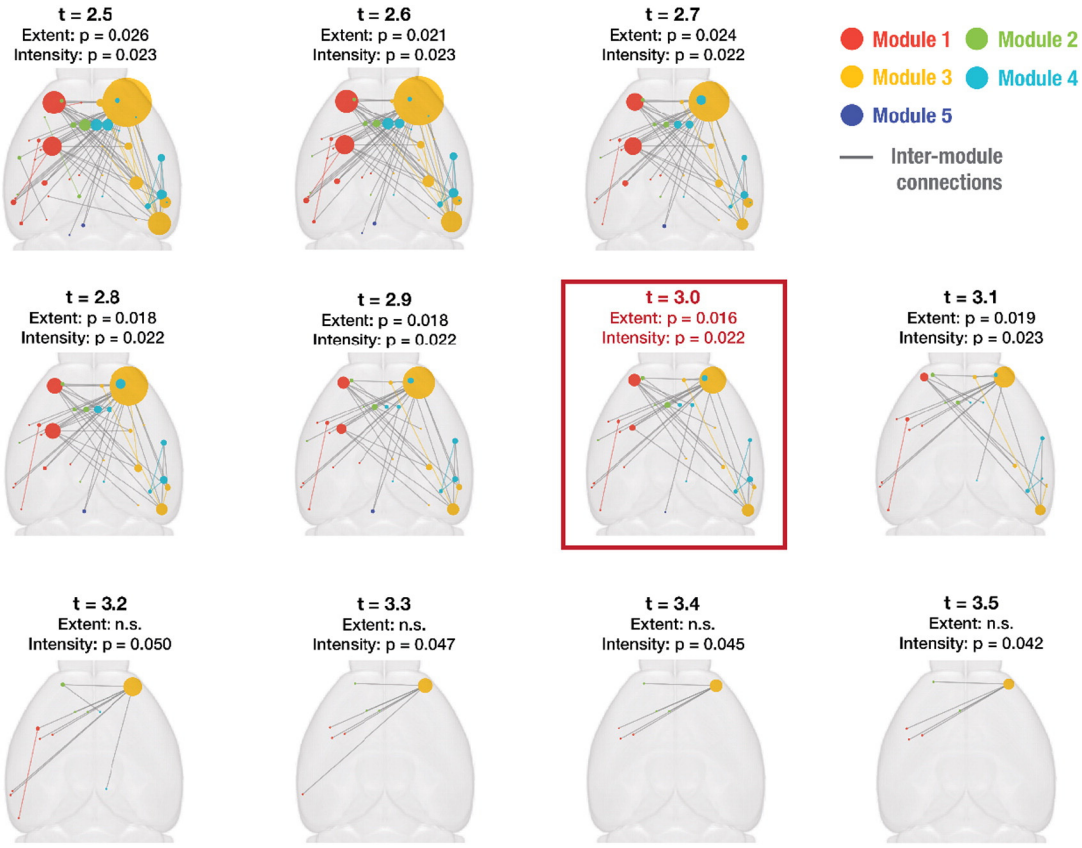

Fig. 5. Network Based Statistics analyses under different primary thresholds. Network Based Statistics (NBS) requires a primary threshold to construct a set of suprathreshold links for later permutation testing. A range of primary thresholds were examined from t = 2.5 to t = 3.5, and the threshold (t = 3.0) results in a components with the highest statistical significance. Meanwhile, two different measures can be used for the NBS. One is the component extent that is the total number of connections the component comprises, and the other is the component intensity that is the sum of test statistic values across all connections comprising the component (Zalesky et al., 2010). Size of a node represents the number of abnormal connections associated with that node. Color of a node represents the module to which it belongs. Colored lines are the abnormal within-module connections, and gray lines are the abnormal inter-module connections. All colors are determined by the modularity analysis on the averaged connectivity matrix across subjects, and are used for the purpose of demonstration only.

3.4. Abnormal white matter tracts contribute to abnormal structural connectomes

The dorsolateral orbitofrontal cortex was the most affected region in the structural connectome. By combining results of probabilistic tractography and neural-tracing data of Allen Brain Altas (*http://connectivity.brain-map.org/*), we investigated structural connectivity profiles of the dorsolateral orbitofrontal cortex, and identified two major white matter tracts (Fig. 8), including 1) the forceps minor, which connects the two hemispheres of the prefrontal regions *via* the genu of the corpus callosum; and 2) the lateral-cortical tracts, which pass through a collection of lateral cortical regions.

We reconstructed the forceps minor and lateral-cortical tracts using probabilistic tractography and compared average diffusion-tensor properties between two groups for each tract. Socially isolated mice showed significantly higher fractional anisotropy ($t(29.06) = -2.45$, $p = 0.021$, uncorrected) and lower radial diffusivity ($t(24.90) = 2.41$, $p = 0.023$, uncorrected) in the forceps minor (Fig. 9A). No significant difference were observed in mean diffusivity ($t(26.07) = 1.27$, $p = 0.22$, uncorrected) and axial diffusivity ($t(28.43) = 0.25$, $p = 0.80$,

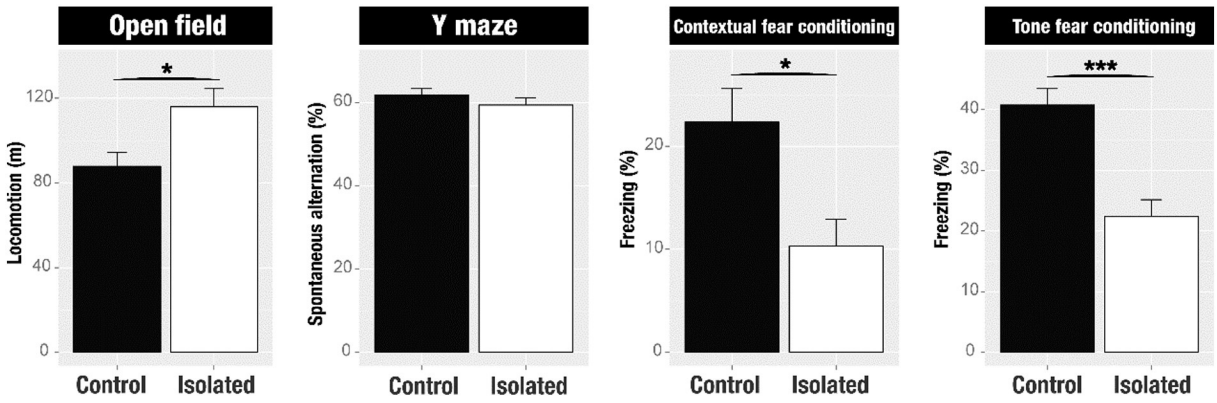

Fig. 6. Social-isolated mice show hyper-locomotor activities and deficits in fear conditioning. Values are presented as mean ± SEM for each group. *p < 0.05, **p < 0.01, and ***p < 0.001.

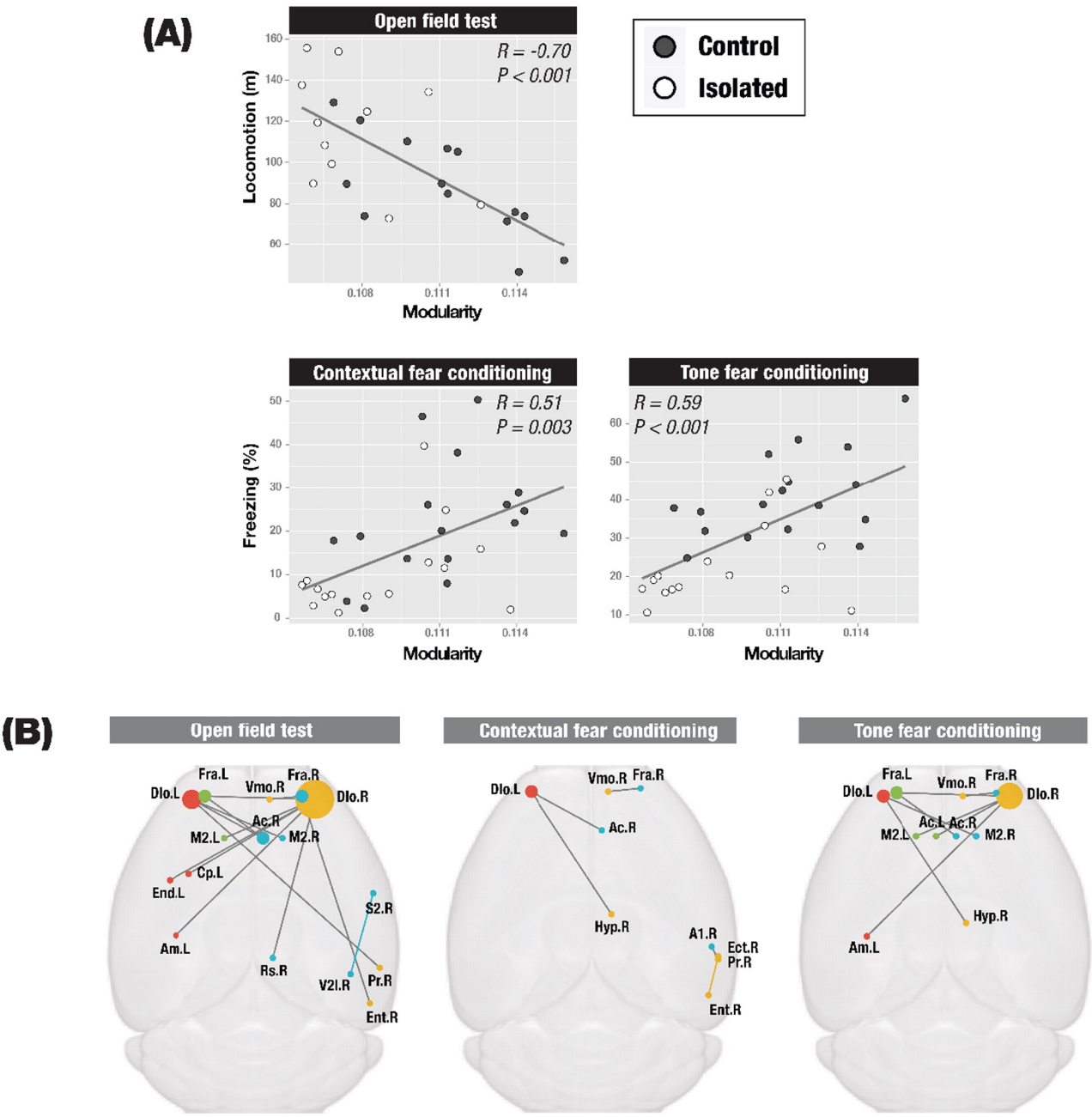

Fig. 7. Structural connectome is correlated with behavioral performances. (A) The network properties that are correlated with behaviors. Modularity is significantly correlated with locomotor activities and fear conditioning (B) The abnormal connections are correlated with locomotor activities and fear conditioning. The full name of each abbreviation is listed in Supplementary Table S1, and the correlations of each connection are listed in Supplementary Table S2.

uncorrected) of the forceps minor. Radial diffusivity of the left lateral-cortical tracts was significantly lower in the socially isolated mice (Fig. 9A, $t(28.60) = 2.20$, $p = 0.036$, uncorrected), but this was not the case for the right lateral-cortical tracts ($t(29.94) = 1.51$, $p = 0.14$, uncorrected) although the patterns of changes were similar. Lateral-cortical tracts showed no significant difference in fractional anisotropy, mean and axial diffusivities ($p > 0.05$, uncorrected). As the size of white matter tracts may affect the estimation of diffusion-tensor properties, we also compared the volume of these tracts and found no significant difference between groups ($p > 0.05$, uncorrected).

Diffusion MRI revealed microstructural changes in the forceps minor and the lateral-cortical tracts that were induced by social isolation. We performed Immunohistochemical analyses to investigate the microscopic structural changes that could underlie the diffusion MRI findings. We targeted at the forceps minor, because 1) the lateral-cortical tracts are a collection of fibers that are too extensive to be sampled; 2) as a part of the corpus callosum, the forceps minor is an white matter bundle that covers a few brain sections and can be accurately sampled in histological experiments; and 3) the corpus callosum has been well studied for both its structure and function and is the most commonly used "model" in diffusion MRI research. The density of total cells (DAPI+) and oligodendrocytes (CC1+/Olig2+), and the intensity of myelin basic protein (MBP+) were measured in the forceps minor (Fig. 9B). The socially isolated mice had significantly higher cell density (Fig. 9C; $t(10.99) = -7.22$, $p < 0.001$, uncorrected) than the controls. As the dominant cell type in the forceps minor (>80% of the total), oligodendrocytes were also present at a significantly higher density in the socially isolated mice (Fig. 9C; $t(8.68) = -2.63$, $p = 0.028$, uncorrected). We did not observe any difference in the intensity of myelin basic protein (Fig. 9C; $t(10.83) = -0.27$, $p = 0.79$, uncorrected).

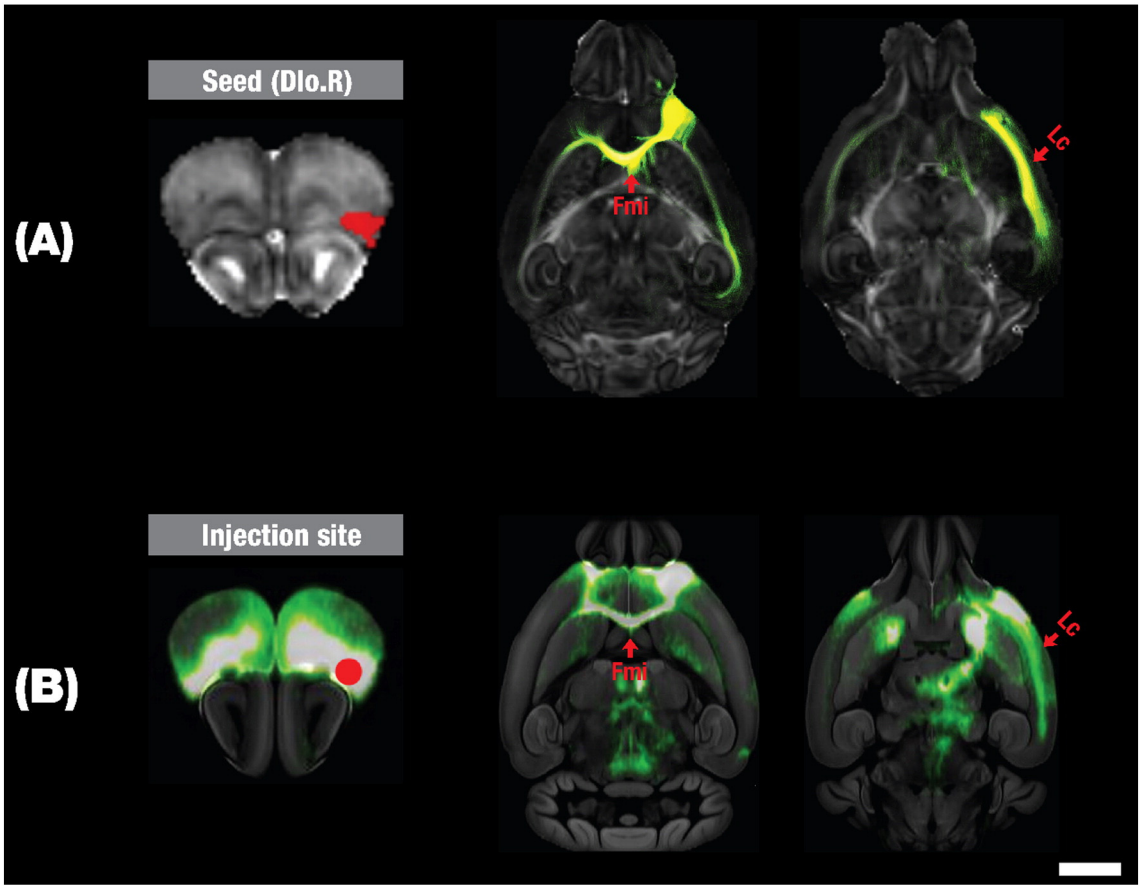

Fig. 8. The structural connectivity profiles of the dorsolateral orbitofrontal cortex. (A) Probabilistic tractography from the seed of the right dorsolateral orbitofrontal cortex (Dlo.R). (B) Axonal projection mapping of the Dlo.R in C57BL/6 mice from the Mouse Connectivity database of Allen Brain Atlas (http://connectivity.brain-map.org/). Note that the Allen Brain atlas has different cortical parcellations to the CAI atlas (Ullmann et al., 2013). We selected an injection site (red dot) that was closest to the Dlo.R. Both probabilistic tractography and axonal projection mapping reveal two major tracts of Dlo.R, including the forceps minor (Fmi) and lateral-cortical tracts (Lc). Scale bar = 2 mm.

4. Discussion

Based on diffusion MRI and probabilistic tractography, we have identified the abnormal patterns in the structural connectome of socially isolated mice, characterized by reduced modularity and increased inter-hemispheric connections from prefrontal regions. These abnormalities were correlated with behavioral deficits caused by the social isolation, and the white matter changes in the forceps minor and lateral-cortical tracts contributed to the abnormal connectome. These results suggest that social experience during adolescence is an important modulator of the structural connectome.

4.1. Orbitofrontal cortex, white matter tracts and abnormal structural connectome

The most distinct features of the abnormal connectome were the abnormalities associated with the dorsolateral orbitofrontal cortex (Dlo). Most of the abnormal edges were connected to the Dlo (Fig. 4). With higher connectivity probabilities in the socially isolated mice, these abnormal edges caused the higher nodal degree in the Dlo as well as in the entorhinal cortex and perirhinal cortex that were connected with Dlo (Fig. 3 and Supplementary Figure S5). Abnormal edges from the Dlo may also reduce the modularity in socially isolated mice (Fig. 2). Generally, a network with high modularity has dense within-module connections, but sparse between-module connections. Most of the abnormal edges were inter-modular or inter-hemispheric (Fig. 4), which tended to increase the between-module connections and reduce the modularity in socially isolated mice. Based on the above observations, we believe that the changes in the Dlo and its neural pathways, including the forceps minor and lateral-cortical tracts (Fig. 8), may be the main contributor to the abnormal structural connectome of socially isolated mice.

Tractography-based analyses and histological examinations revealed microstructures changes in these tracts, which were characterized by an increase in fractional anisotropy (for the forceps minor) and a decrease in radial diffusivity (for the forceps minor and lateral-cortical tracts). Targeting the forceps minor, we revealed an increase of cell density in the socially isolated mice, which could hinder the diffusion of water and contribute to the alterations in fractional anisotropy and radial diffusivity. We didn't observe significant changes in axial diffusivity, indicating that most cells in the forceps minor are aligned in parallel to the tract rather than randomly aligned. Supporting this assumption, the majority of cells in the forceps minor are oligodendrocytes, which tend to be aligned along axons (Baumann and Pham-Dinh, 2001). These changes in diffusion-tensor properties and oligodendrocytes indicate a change in myelination (Zhang J et al. 2012). However, we didn't observe any significant changes in the intensity of myelin basic protein (MBP). Two factors may explain this; first, the intensity of MBP staining cannot be used to adequately quantify the level of myelination. Although the antibody against MBP is commonly used to localize myelin, the intensity of staining decreases when compact myelin sheaths are present, as MBP in sheaths is less accessible to antibodies (Sternberger et al., 1978). Thus, we cannot draw a conclusion about the amount of myelination solely based on the current evidence. Second, the forceps minor has the high density of small axons and large proportion of unmyelinated axons (Lamantia and Rakic, 1990; Aboitiz et al., 1992). Meanwhile, the high density of axons is likely associated

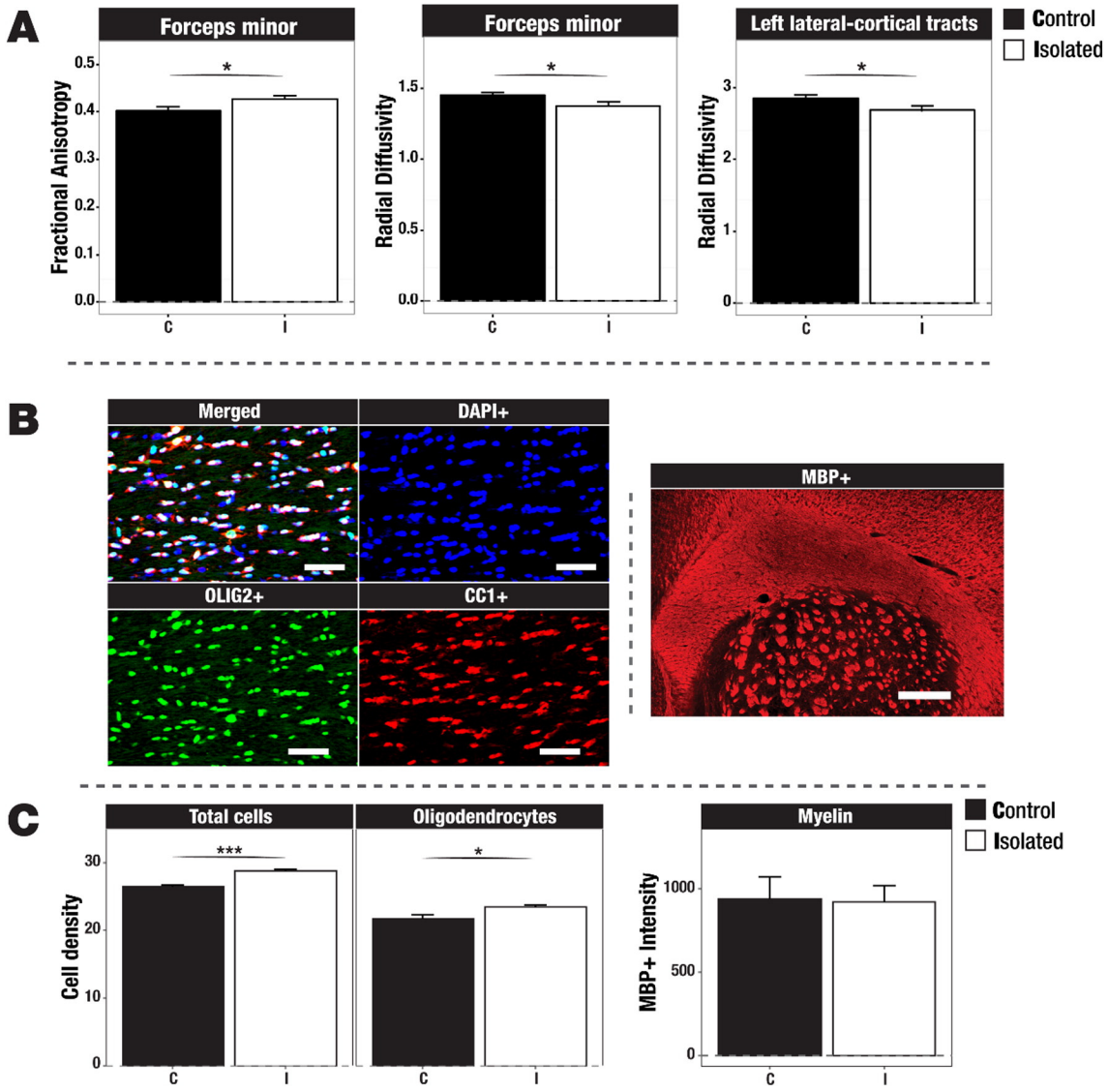

Fig. 9. Abnormal white matter microstructures in socially-isolated mice. (A) Diffusion MRI detects abnormalities in the forceps minor and lateral-cortical tracts of socially isolated mice. The unit of radial diffusivity is $\times 10^{-4}$ mm^2/s. (B) Representative immunofluorescence images of the forceps minor for DAPI+ (blue, all cells), Olig2+ (green, oligodendrocytes and oligodendrocytes lineage cells), and CC1+ (red, mature oligodendrocytes) viewed with a 20× objective (scale bar = 50 μm), and MBP+ (red, myelin basic protein) using a 10× objective (scale bar = 300 μm). More representative immunofluorescence images were provided in Supplementary Figure S6. (C) Socially isolated mice have a significantly higher density of total cells (DAPI+) and oligodendrocytes (OLIG2+/CC1+) than the controls. The units of cell density is cells/10^{4}μm^2. Values are presented as mean ± SEM.

with a high density of oligodendrocytes (Simons and Trajkovic, 2006). Thus, the change in the oligodendrocytes may be more substantial than the change in myelination.

We observed several "lateralized" changes in the socially-isolated mice. The left lateral-cortical tracts showed significant abnormalities in the white matter microstructures (Fig. 9), whereas the right lateral-cortical tracts displayed a similar trend but not as significant as the left tracts. Meanwhile, we identified more abnormal inter-hemispheric edges that connected the right Dlo with brain regions of left hemisphere than the abnormal edges connecting left Dlo with right hemisphere (Fig. 4). These "lateralized" changes were consistent with each other, as these edges connecting right Dlo with left hemisphere had to pass through abnormal left lateral-cortical tracts. These asymmetric changes may be caused by structural and functional asymmetries of the brain regions connected by the tracts. For example, the rodent hippocampus has asymmetric spine morphology, glutamate receptor distribution and synaptic plasticity (Kawakami et al., 2003; Kohl et al., 2011; Shinohara et al., 2008). In addition, hippocampal long-term memory processing is lateralized in mice, as silencing the left hippocampus impairs long-term memory, whereas silencing the right hippocampus does not (Shipton et al., 2014). Since lateral-cortical tracts connect the entorhinal-hippocampal system, the asymmetries of the hippocampus may contribute to the asymmetric changes of these tracts. However, besides the asymmetries of the hippocampus, we know few about the structural and functional asymmetries in rodent brains, and therefore, the above explanations on our "lateralized" findings requires further investigation.

4.2. Orbitofrontal cortex, social experience and axonal pruning

The orbitofrontal cortex is a key brain region essential for social-emotional behaviors (Adolphs, 2001). The development of the orbitofrontal cortex and its neural pathways is influenced and modulated by environmental changes. During adolescence, the major change is a dramatic transition in social roles from dependent juveniles into independent adults (Smetana et al., 2006). Here, we demonstrated that the orbitofrontal cortex and its connections were particularly sensitive to the effect of adolescent social isolation, suggesting that social

experience is essential for the structural remodelling of social-emotional circuitry. Without social experience, the structural remodelling of the orbitofrontal cortex and its neural pathways may be disrupted, resulting in an abnormal structural connectome.

Axonal pruning may be one component of disrupted structural remodelling in the orbitofrontal cortex. During early brain development, the brain generates exuberant immature projections (Low and Cheng, 2006). Many of these immature axons are pruned or eliminated during postnatal development, with the remaining connections maintained to form functioning circuits (Cressman et al., 2010; Low and Cheng, 2006). Pruning of axons are experience-induced and are largely shaped by environmental influences (Blakemore, 2008). Since social experience is the major environmental stimulus during adolescent development, social deprivation may disrupt the normal axonal pruning of neural pathways involving the orbitofrontal cortex, leaving socially isolated animals with overabundant immature axons. These immature axons tend to increase connectivity probabilities and thus increase the network degree of the affected regions. The organization of immature axons may also affect the modularity and small-worldness of neural structures. From adolescence to young adulthood, axonal pruning mainly occurs in the prefrontal regions and related pathways (Cressman et al., 2010; Koss et al., 2014). In line with this, the prefrontal cortex, especially the orbitofrontal cortex, becomes the most affected region in the structural connectome of socially isolated mice. Meanwhile, the changes in axons may be accompanied by other remodelling events, including oligodendrocytes maturation and myelination (Fields, 2010; Simons and Trajkovic, 2006). These changes may compose the biological basis of the abnormal structural connectome in the socially isolated mice, and worth investigation in the future.

4.3. Structural connectome and behavioral deficits

The abnormal structural connectome of socially isolated mice may account for their behavioral deficits. Network properties, especially modularity, displayed strong correlations with both fear memory and locomotor activities (Fig. 7A). As the modularity of mice brain networks increases as the mice mature (Ingalhalikar et al., 2015), the lower modularity of socially isolated mice indicates that their brain circuits for these behaviors may be not fully matured. This strong association suggests that the structural connectome is an important *endo*-phenotype that provides a link between brain abnormalities and behavioral deficits.

In addition to whole brain properties, we also identified connection-wise correlations in brain regions that were highly related to fear memory (Fig. 7B). Most of these connections are linked to the key regions of fear memory circuits, including the prefrontal regions (Dlo, Vmo, and Fra), anterior cingulate cortex, hypothalamus, and amygdala. We also observed correlations between fear memory and connections of the ectorhinal, perirhinal, and entorhinal cortices. As important cortical interfaces of limbic systems, these regions receive information from all sensory regions and have extensive reciprocal connections with the amygdala, hippocampus, and prefrontal regions (Burwell et al., 1995; Majak and Pitkanen, 2003; McDonald and Mascagni, 1997; Pitkanen et al., 2000; Swanson and Cowan, 1977). Inactivation or lesions of these regions impair normal functions of fear learning and memory (Baldi and Bucherelli, 2014; Baldi and Bucherelli, 2015; Baldi et al., 2013; Burwell et al., 2004; Corodimas and LeDoux, 1995; Hebert and Dash, 2004; Howse et al., 2003; Ji and Maren, 2008; Majak and Pitkanen, 2003; Maren and Fanselow, 1997; Sacchetti et al., 1999). Their structural connectivity and functions explain their correlations with fear memory. Connection-wise correlations with locomotor activities are more widespread than those with fear memory, as more regions and connections may affect general locomotor functions. Interestingly, none of these connection-wise correlations are higher or more significant than the network-wise correlation for modularity (Fig. 7A and Supplementary Table S2), indicating that the overall structural connectome can explain more of the individual variance in behavioral performances than any single connection.

4.4. Limitation and future direction

The main technique used in this study was diffusion MRI. This powerful imaging technique helped us to identify microstructural changes in the white matter of socially isolated mice, which contributed to the abnormalities in the structural connectome. As diffusion MRI visualizes biological tissues by mapping the diffusion of water molecules of tissues (Johansen-Berg and Behrens, 2013; Mori and Zhang, 2006), the diffusion-tensor properties lack sensitivity and only indirectly reflect microstructural changes to tissues, and therefore cannot directly pinpoint the pathology. To overcome this limitation, we need to resort to other techniques to scrutinize the non-specific findings revealed by diffusion MRI. We performed immunohistochemical analyses and proved that the changes in diffusion-tensor properties were not false-positive, but changes in axons and myelination were not directly investigated. Future studies utilizing more specific imaging techniques, such as electron microscopy, will help to fully characterize white matter microstructural changes in axons and myelination.

Another limitation of this study was the "*ex-vivo*" scanning. Diffusion MRI technique is well-known for its "non-invasive" and "*in-vivo*" mapping of white matter structures and structural connectome. The "non-invasive" feature allows longitudinal scanning, which is useful for studying the development and changes of structural connectome. In addition, "*in-vivo*" scanning with functional MRI is commonly used to map functional connectivity and functional connectome, which is an important complement to structural connectome (Smith et al., 2013; Sporns, 2013). However, we failed to take advantage of the "non-invasive" aspect of MRI techniques, as our animals were perfused and specimens were subsequently scanned. Due to the small size of the mouse brain, images with a high spatial resolution are required to delineate the microstructures of the brain (Zhang et al., 2012), which makes the "*in-vivo*" scanning of mice brains quite challenging. Meanwhile, the animal ethics requirement that living animals cannot be anesthetized too long poses another challenge for acquiring high-resolution *in-vivo* diffusion images. Thus, we resorted to *ex-vivo* diffusion MRI as with the resolution afforded by the technique (0.1 mm^3) we were able to characterize major white matter tracts in the mouse brain.

In conclusion, adolescent social isolation disrupts the structural connectome of mice, characterized by decreased modularity and abnormal inter-hemispheric connections from the orbitofrontal cortex. The altered structural connectome is mainly contributed by abnormal neural pathways of the orbitofrontal cortex, including the forceps minor and lateral cortical tracts, the cellular basis of which warrants further investigation in the future.

Conflict of Interest

The authors declare no competing financial interests.

Acknowledgements

This work was supported by the National Basic Research Program of China (973 program; 2011CB707800), the Strategic Priority Research Program of the Chinese Academy of Sciences (Grant No. XDB02030300), the Natural Science Foundation of China (91132301), and a National Health and Medical Research Council (NHMRC) Australia project grant 1043045 (LJR). LJR is supported by an NHMRC Principal Research Fellowship and TJE is supported by a PhD student Australian Postgraduate Award from the Australian Government. We thank the Queensland State Government for support of the 16.4T through the Queensland NMR Network, and thank Dr. Alan Woodruff for language editing.

Appendix A. Supplementary data

Supplementary material.

References

Aboitiz, F., Scheibel, A.B., Fisher, R.S., Zaidel, E., 1992. Fiber composition of the human corpus callosum. Brain Res. 598, 143–153.

Adolphs, R., 2001. The neurobiology of social cognition. Curr. Opin. Neurobiol. 11, 231–239.

Baldi, E., Bucherelli, C., 2014. Entorhinal cortex contribution to contextual fear conditioning extinction and reconsolidation in rats. Neurobiol. Learn. Mem. 110, 64–71.

Baldi, E., Bucherelli, C., 2015. Brain sites involved in fear memory reconsolidation and extinction of rodents. Neurosci. Biobehav. Rev. 53, 160–190.

Baldi, E., Liuzzo, A., Bucherelli, C., 2013. Fimbria-fornix and entorhinal cortex differential contribution to contextual and cued fear conditioning consolidation in rats. Physiol. Behav. 114–115, 42–48.

Baumann, N., Pham-Dinh, D., 2001. Biology of oligodendrocyte and myelin in the mammalian central nervous system. Physiol. Rev. 81, 871–927.

Blakemore, S.J., 2008. The social brain in adolescence. Nat. Rev. Neurosci. 9, 267–277.

Blakemore, S.J., Mills, K.L., 2014. Is adolescence a sensitive period for sociocultural processing? Annu. Rev. Psychol. 65 (65), 187–207.

Brandes, U., 2001. A faster algorithm for betweenness centrality*. J. Math. Sociol. 25, 163–177.

Burwell, R.D., Witter, M.P., Amaral, D.G., 1995. Perirhinal and postrhinal cortices of the rat: a review of the neuroanatomical literature and comparison with findings from the monkey brain. Hippocampus 5, 390–408.

Burwell, R.D., Saddoris, M.P., Bucci, D.J., Wiig, K.A., 2004. Corticohippocampal contributions to spatial and contextual learning. J. Neurosci. 24, 3826–3836.

Buwalda, B., Geerdink, M., Vidal, J., Koolhaas, J.M., 2011. Social behavior and social stress in adolescence: a focus on animal models. Neurosci. Biobehav. Rev. 35, 1713–1721.

Calamante, F., Tournier, J.D., Kurniawan, N.D., Yang, Z., Gyengesi, E., Galloway, G.J., Reutens, D.C., Connelly, A., 2012. Super-resolution track-density imaging studies of mouse brain: comparison to histology. NeuroImage 59, 286–296.

Chuang, N., Mori, S., Yamamoto, A., Jiang, H., Ye, X., Xu, X., Richards, L.J., Nathans, J., Miller, M.I., Toga, A.W., Sidman, R.L., Zhang, J., 2011. An MRI-based atlas and database of the developing mouse brain. NeuroImage 54, 80–89.

Clauset, A., Newman, M.E.J., Moore, C., 2004. Finding community structure in very large networks. Phys. Rev. E 70.

Corodimas, K.P., LeDoux, J.E., 1995. Disruptive effects of posttraining perirhinal cortex lesions on conditioned fear: contributions of contextual cues. Behav. Neurosci. 109, 613–619.

Cressman, V.L., Balaban, J., Steinfeld, S., Shemyakin, A., Graham, P., Parisot, N., Moore, H., 2010. Prefrontal cortical inputs to the basal amygdala undergo pruning during late adolescence in the rat. J. Comp. Neurol. 518, 2693–2709.

Danon, L., Diaz-Guilera, A., Arenas, A., 2006. The effect of size heterogeneity on community identification in complex networks. J. Stat. Mech.: Theory Exp.

Dember, W.N., Fowler, H., 1958. Spontaneous alternation behavior. Psychol. Bull. 55, 412–428.

Fields, R.D., 2010. Neuroscience. Change in the brain's white matter. Science 330, 768–769.

Fuhrmann, D., Knoll, L.J., Blakemore, S.J., 2015. Adolescence as a sensitive period of brain development. Trends Cogn. Sci. 19, 558–566.

Girvan, M., Newman, M.E.J., 2002. Community structure in social and biological networks. Proc. Natl. Acad. Sci. U. S. A. 99, 7821–7826.

Griffa, A., Baumann, P.S., Thiran, J.P., Hagmann, P., 2013. Structural connectomics in brain diseases. NeuroImage 80, 515–526.

Hebert, A.E., Dash, P.K., 2004. Plasticity in the entorhinal cortex suppresses memory for contextual fear. J. Neurosci. 24, 10111–10116.

Holm, S., 1979. A simple sequentially rejective multiple test procedure. Scand. J. Stat. 6, 65–70.

Howse, D.J., Squires, A.S., Martin, G.M., Skinner, D.M., 2003. Perirhinal cortex lesions impair context aversion learning. Learn. Mem. 10, 161–167.

Ingalhalikar, M., Parker, D., Ghanbari, Y., Smith, A., Hua, K., Mori, S., Abel, T., Davatzikos, C., Verma, R., 2015. Connectome and maturation profiles of the developing mouse brain using diffusion tensor imaging. Cereb. Cortex 25, 2696–2706.

Ji, J., Maren, S., 2008. Lesions of the entorhinal cortex or fornix disrupt the context-dependence of fear extinction in rats. Behav. Brain Res. 194, 201–206.

Johansen-Berg, H., Behrens, T.E., 2013. Diffusion MRI: from quantitative measurement to in vivo neuroanatomy. Academic Press.

Kawakami, R., Shinohara, Y., Kato, Y., Sugiyama, H., Shigemoto, R., Ito, I., 2003. Asymmetrical allocation of NMDA receptor epsilon2 subunits in hippocampal circuitry. Science 300, 990–994.

Kohl, M.M., Shipton, O.A., Deacon, R.M., Rawlins, J.N., Deisseroth, K., Paulsen, O., 2011. Hemisphere-specific optogenetic stimulation reveals left-right asymmetry of hippocampal plasticity. Nat. Neurosci. 14, 1413–1415.

Koss, W.A., Belden, C.E., Hristov, A.D., Juraska, J.M., 2014. Dendritic remodeling in the adolescent medial prefrontal cortex and the basolateral amygdala of male and female rats. Synapse 68, 61–72.

Lamantia, A.S., Rakic, P., 1990. Cytological and quantitative characteristics of four cerebral commissures in the rhesus monkey. J. Comp. Neurol. 291, 520–537.

Latora, V., Marchiori, M., 2003. Economic small-world behavior in weighted networks. Eur. Phys. Jo. B 32, 249–263.

Liu, J., Dietz, K., DeLoyht, J.M., Pedre, X., Kelkar, D., Kaur, J., Vialou, V., Lobo, M.K., Dietz, D.M., Nestler, E.J., Dupree, J., Casaccia, P., 2012. Impaired adult myelination in the prefrontal cortex of socially isolated mice. Nat. Neurosci. 15, 1621–1623.

Low, L.K., Cheng, H.J., 2006. Axon pruning: an essential step underlying the developmental plasticity of neuronal connections. Philos. Trans. R. Soc., B 361, 1531–1544.

Majak, K., Pitkanen, A., 2003. Activation of the amygdalo-entorhinal pathway in fear-conditioning in rat. Eur. J. Neurosci. 18, 1652–1659.

Makinodan, M., Rosen, K.M., Ito, S., Corfas, G., 2012. A critical period for social experience-dependent oligodendrocyte maturation and myelination. Science 337, 1357–1360.

Maren, S., 2001. Neurobiology of Pavlovian fear conditioning. Annu. Rev. Neurosci. 24, 897–931.

Maren, S., Fanselow, M.S., 1997. Electrolytic lesions of the fimbria/fornix, dorsal hippocampus, or entorhinal cortex produce anterograde deficits in contextual fear conditioning in rats. Neurobiol. Learn. Mem. 67, 142–149.

Maslov, S., Sneppen, K., 2002. Specificity and stability in topology of protein networks. Science 296, 910–913.

McDonald, A.J., Mascagni, F., 1997. Projections of the lateral entorhinal cortex to the amygdala: a *Phaseolus vulgaris* leucoagglutinin study in the rat. Neuroscience 77, 445–459.

Moldrich, R.X., Pannek, K., Hoch, R., Rubenstein, J.L., Kurniawan, N.D., Richards, L.J., 2010. Comparative mouse brain tractography of diffusion magnetic resonance imaging. NeuroImage 51, 1027–1036.

Mori, S., Zhang, J., 2006. Principles of diffusion tensor imaging and its applications to basic neuroscience research. Neuron. 51, 527–539.

Pattwell, S.S., Bath, K.G., Casey, B.J., Ninan, I., Lee, F.S., 2011. Selective early-acquired fear memories undergo temporary suppression during adolescence. Proc. Natl. Acad. Sci. U. S. A. 108, 1182–1187.

Pitkanen, A., Pikkarainen, M., Nurminen, N., Ylinen, A., 2000. Reciprocal Connections Between the Amygdala and the Hippocampal Formation, Perirhinal Cortex, and Postrhinal Cortex in rat - A Review. Parahippocampal Region. 911 pp. 369–391.

Rubinov, M., Sporns, O., 2010. Complex network measures of brain connectivity: uses and interpretations. NeuroImage 52, 1059–1069.

Sacchetti, B., Lorenzini, C.A., Baldi, E., Tassoni, G., Bucherelli, C., 1999. Auditory thalamus, dorsal hippocampus, basolateral amygdala, and perirhinal cortex role in the consolidation of conditioned freezing to context and to acoustic conditioned stimulus in the rat. J. Neurosci. 19, 9570–9578.

Schindelin, J., Arganda-Carreras, I., Frise, E., Kaynig, V., Longair, M., Pietzsch, T., Preibisch, S., Rueden, C., Saalfeld, S., Schmid, B., Tinevez, J.Y., White, D.J., Hartenstein, V., Eliceiri, K., Tomancak, P., Cardona, A., 2012. Fiji: an open-source platform for biological-image analysis. Nat. Methods 9, 676–682.

Shinohara, Y., Hirase, H., Watanabe, M., Itakura, M., Takahashi, M., Shigemoto, R., 2008. Left-right asymmetry of the hippocampal synapses with differential subunit allocation of glutamate receptors. Proc. Natl. Acad. Sci. U. S. A. 105, 19498–19503.

Shipton, O.A., El-Gaby, M., Apergis-Schoute, J., Deisseroth, K., Bannerman, D.M., Paulsen, O., Kohl, M.M., 2014. Left-right dissociation of hippocampal memory processes in mice. Proc. Natl. Acad. Sci. U. S. A. 111, 15238–15243.

Simons, M., Trajkovic, K., 2006. Neuron-glia communication in the control of oligodendrocyte function and myelin biogenesis. J. Cell Sci. 119, 4381–4389.

Smetana, J.G., Campione-Barr, N., Metzger, A., 2006. Adolescent development in interpersonal and societal contexts. Annu. Rev. Psychol. 57, 255–284.

Smith, S.M., Beckmann, C.F., Andersson, J., Auerbach, E.J., Bijsterbosch, J., Douaud, G., Duff, E., Feinberg, D.A., Griffanti, L., Harms, M.P., Kelly, M., Laumann, T., Miller, K.L., Moeller, S., Petersen, S., Power, J., Salimi-Khorshidi, G., Snyder, A.Z., Vu, A.T., Woolrich, M.W., Xu, J.Q., Yacoub, E., Ugurbil, K., Van Essen, D.C., Glasser, M.F., Consortium, W.-M.H., 2013. Resting-state fMRI in the human connectome project. NeuroImage 80, 144–168.

Sporns, O., 2013. Structure and function of complex brain networks. Dialogues Clin. Neurosci. 15, 247–262.

Sporns, O., Tononi, G., Kotter, R., 2005. The human connectome: a structural description of the human brain. PLoS Comput. Biol. 1, 245–251.

Sternberger, N.H., Itoyama, Y., Kies, M.W., Webster, H.D., 1978. Myelin basic protein demonstrated immunocytochemically in oligodendroglia prior to myelin sheath formation. Proc. Natl. Acad. Sci. USA 75, 2521–2524.

Swanson, L.W., Cowan, W.M., 1977. An autoradiographic study of the organization of the efferent connections of the hippocampal formation in the rat. J. Comp. Neurol. 172, 49–84.

Tournier, J.D., Calamante, F., Connelly, A., 2007. Robust determination of the fibre orientation distribution in diffusion MRI: non-negativity constrained super-resolved spherical deconvolution. NeuroImage 35, 1459–1472.

Ullmann, J.F., Watson, C., Janke, A.L., Kurniawan, N.D., Reutens, D.C., 2013. A segmentation protocol and MRI atlas of the C57BL/6J mouse neocortex. NeuroImage 78, 196–203.

Walsh, R.N., Cummins, R.A., 1976. The open-field test: a critical review. Psychol. Bull. 83, 482–504.

Wang, J.H., Wang, X.D., Xia, M.R., Liao, X.H., Evans, A., He, Y., 2015. GRETNA: a graph theoretical network analysis toolbox for imaging connectomics. Front. Hum. Neurosci. 9.

Watts, D.J., Strogatz, S.H., 1998. Collective dynamics of 'small-world' networks. Nature 393, 440–442.

Zalesky, A., Fornito, A., Bullmore, E.T., 2010. Network-based statistic: identifying differences in brain networks. NeuroImage 53, 1197–1207.

Zhang, J., Aggarwal, M., Mori, S., 2012. Structural insights into the rodent CNS via diffusion tensor imaging. Trends Neurosci. 35, 412–421.

Zuo, N.M., Cheng, J., Jiang, T.Z., 2012. Diffusion magnetic resonance imaging for Brainnetome: a critical review. Neurosci. Bull. 28, 375–388.